Design and analysis of the magnetic suspension system in an energy storage flywheel

Arunvel Kailasan*
University of Virginia
Charlottesville - VA , USA

Wei Jiang
University of Virginia
Charlottesville - VA , USA

Timothy Dimond
University of Virginia
Charlottesville - VA , USA

David Sheffler
University of Virginia
Charlottesville - VA , USA

Paul Allaire
University of Virginia
Charlottesville - VA , USA

Abstract

Over the past decade, there has been a rising need to develop more efficient, sustainable and environmentally friendly means of short term energy storage. Flywheel energy storage systems store kinetic energy by continuously spinning a compact rotor in a low-friction environment. Magnetic bearing suspension systems are desirable for this application since they significantly increase efficiency, reduce waste heat when operated in vacuum and reduce power requirements for the electronics. A demonstration flywheel energy storage test rig under development at the University of Virginia will use a five-axis active magnetic bearing support system. This paper discusses the design and analysis procedure of the flywheel magnetic suspension system. The magnetic suspension system will be controlled by a μ-synthesis controller, with an adaptive auto-balancing algorithm. Preliminary calculations are performed to determine the various design parameters such as nominal air gap, number of coil turns required, and stator/rotor diameter and thickness using linear magnetic circuit models. Finally, a 3-dimensional finite element analysis was conducted with commercial finite element software to verify the calculated design parameters. The flux path was visualized for both the thrust and radial magnetic bearings and important parameters such as load capacity, flux density, inductance and slew rate were calculated.

1 Introduction

Flywheels have gained importance in short term energy storage due to their high energy densities and smaller footprint [1,2]. Flywheel energy storage systems store kinetic energy by continuously spinning a compact rotor in a low-friction environment. The kinetic energy of the flywheel is $\frac{1}{2} J_p \Omega^2$, where J_p is the polar mass moment of inertia of the rotor and Ω is the rotational speed. This makes high-speed rotation desirable for energy storage. Recent advances in composite materials has made it possible for a typical flywheel to operate at speeds between 10,000 to 100,000 rpm, depending upon the size and application[3,4]. At such speeds, significant heating due to friction is generated in rolling-element bearings which can result in bearing failure. Moreover, a flywheel has sudden changes in speed when it shifts from the motor mode to the generator mode and vice-versa. Rolling-element bearings, usually, will not be able to respond quickly to this change. For such applications, frictionless non-contact magnetic bearings are ideal [5,6]. Magnetic bearings allow the rotor assembly to rotate at very high speeds with no physical contact with stationary components under normal operating conditions. The reduced losses in the magnetic bearings compared to rolling element bearings increase the overall flywheel efficiency. Typical efficiencies for conversion of mechanical to electrical energy are 95% in flywheel systems. Further, the controller for the bearings can be designed to accommodate sudden speed changes. In addition to these advantages, magnetic bearings do not require lubrication, can operate in vacuum and have very long life periods. All these factors make magnetic bearings a crucial component in a high-efficiency, high rotational-speed flywheel energy storage system design. [7,8]

Design of a magnetic bearing is an integral part of having a good overall flywheel design. This study discusses the design and analysis of the magnetic suspension system of a flywheel under development by the Rotating Machinery and Controls Laboratory (ROMAC) at the University of Virginia. This system comprises of a double-acting thrust bearing and two radial magnetic bearings. Preliminary calculations are performed using linear circuit

*Contact Author Information: ak5xc@virginia.edu, Phone Number, 434-982-2246

models to determine the various design parameters such as air gap; number of coil turns required, stator/rotor diameter and rotor lamination thickness. Finally, a 3-dimensional finite element analysis is conducted in ANSYS to verify the calculated design parameters. The flux path was calculated for both the thrust and radial magnetic bearings and important parameters such as load capacity, flux density, inductance, magnetic energy and slew rate were calculated.

1.1 Flywheel magnetic bearing design

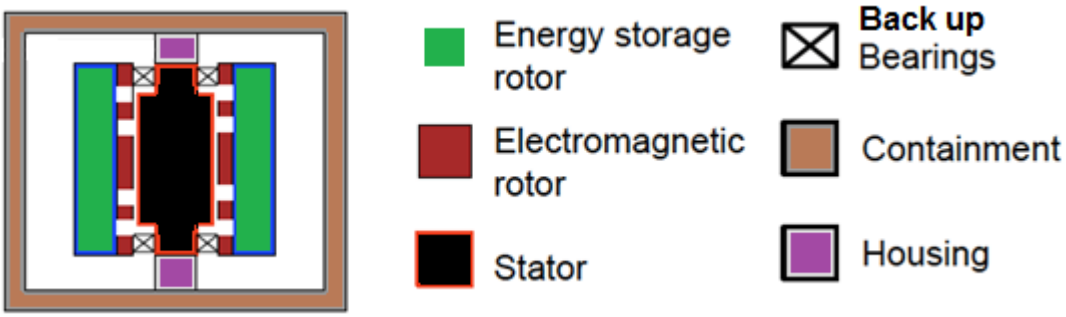

Figure 1: A schematic of the proposed flywheel design [9]

Figure 1 depicts a schematic of the proposed flywheel design. The flywheel is designed to have an energy storage capacity of about 1 kW-hr. This is an inside-out barrel type design in which the stator (shown in black) lies at the center. At the heart of the flywheel energy storage system is an integrated composite rotor (shown in green). This rotor performs the function of the energy storing flywheel as well as the motor/generator system. The rotor is supported with two radial bearings and a double-acting thrust bearing. The design is conceived in such a way that all of the stator components have the same inner diameter. This ensures that they can be attached easily to a single back iron. Similarly, the rotor components are designed to have the same outer diameter. The rotor part of the bearings and the motor-generator system are attached to the composite flywheel with two steel spline rings. The main purpose of this spline ring is to account for high tangential stresses on the composite and to prevent withdrawal of the rotor components when the flywheel rotates at high speed. Four-row tapered rolling element bearings will be used as back up bearings. The entire flywheel energy storage system will be operated in vacuum. This is done to reduce parasitic losses which results in an increase of overall electromechanical efficiency. The weight savings from this type of design can be substantial, and additional advantages include lower component count, reduced material costs, lower mechanical complexity, and reduced manufacturing costs.

In order to have a storage capacity of 1 kW-hr, it was calculated that the composite flywheel should have a height of about 400 mm and a wall thickness of about 100 mm, assuming a carbon-fiber epoxy composite. The polar mass moment inertia of the rotor was then 0.458 kg-m^2. At these dimensions, the flywheel should rotate at a maximum speed of 40,000 rpm and a minimum speed of 20,000 rpm to provide 1 kW-hr of energy storage. These values are used as starting points for the magnetic bearing design.

2 Analysis

This section covers the linear circuit (LC) and finite element analysis (FEA) for the thrust and radial magnetic bearing. Linear circuit models were used for the initial sizing of the double-acting thrust bearing and the radial bearings. These initial designs were then verified using a finite element analysis.

2.1 Thrust Magnetic bearing

A double-acting thrust magnetic bearing was designed for the flywheel. The sectional view of the thrust magnetic bearing is depicted in Figure 2. The main function of the bearing is to levitate the entire flywheel while in operation. The bearing comprises of three major parts: the thrust disk – which is the rotating part of the bearing and is attached to the flywheel, the thrust stator which is attached to the stator back iron and the coils inside the stator. The major function of this thrust bearing is to withstand the weight of the rotor.

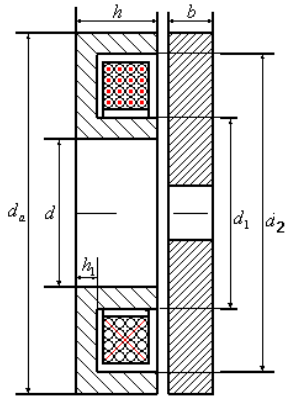

Figure 2 : Sectional view of the thrust magnetic bearing

2.1.1 Linear circuit model

The design load capacity *F* is computed using the total rotor weight and a safety factor. This is expressed as:

$$F = (SF) * mg \tag{1}$$

The design safety factor *SF* accounts for tolerances in the static load capacity, fringing and leaking effects, and unmodeled transient loads. .

The magnetic force in a thrust bearing is given in terms of flux density *B* and pole cross sectional area *A* as:

$$F = \frac{B^2 A}{\mu_0} \tag{2}$$

The flux density can further be written in terms of number of winding turns *N*, current in the coil *I* and air gap *g* as:

$$B = \frac{\mu_0 N i}{2g} \tag{3}$$

Using Eqs. (1-3), the minimum pole cross-sectional area was calculated. The inner and outer diameters of the coil cavity were calculated by keeping constant flux density in the inner and outer poles. This constraint was enforced by forcing the pole face areas to be equal, or:

$$A_a = A_{gi} = A_{go} = \frac{\pi(d_1^2 - d^2)}{4} = \frac{\pi(d_a^2 - {d_2}^2)}{4} \tag{4}$$

Further, the number of turns was calculated based on the maximum current density J_{max}. The maximum current density is a limit commonly employed in industry for coil currents per area to avoid problems associated with coil overheating such as wire insulation break down. This value is usually about 7-9 A/mm^2. The required number of turns is also a function of the peak current I_{max}. The required number of turns is then:

$$N = \frac{A_a J_{\max}}{I_{\max}} \tag{5}$$

Using Eqs. (1–5), the initial sizing was done on the thrust bearing to determine the necessary parameters including pole widths, nominal air gap and number of coil turns. The coil inductance L_c can be approximated as:

$$L_c = \frac{\mu_o N^2 A_a}{2g} \tag{6}$$

And the maximum force slew rate can be calculated as:

$$\frac{dF_{tot}}{dt} = \frac{2I_b V_{\max}}{g_o} \tag{7}$$

2.1.2 Thrust Bearing Finite Element Analysis

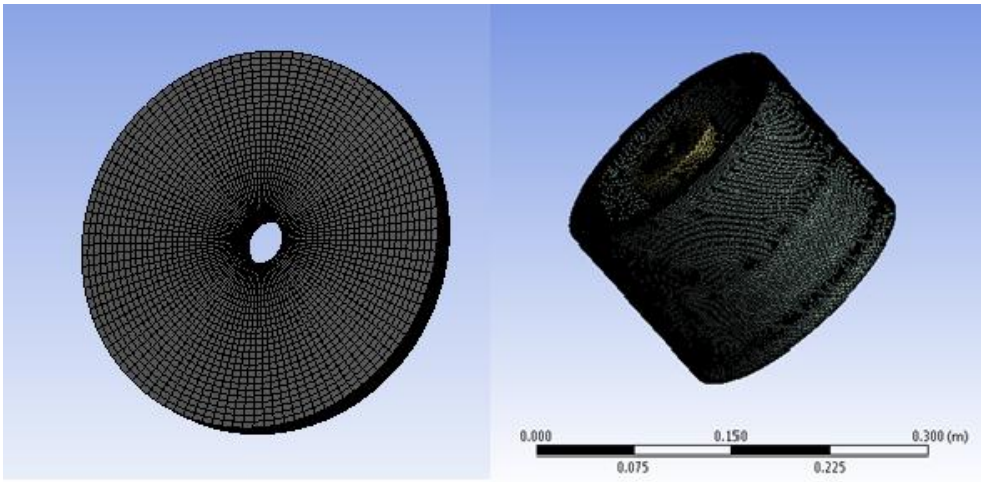

Figure 3: Thrust magnetic bearing model

A three dimensional FEA was conducted to verify the parameters obtained from the linear circuit model of the thrust bearing. ANSYS 11 was used to perform the analysis. A mesh density study was performed to ensure that the results had numerically converged. About 1 million elements were used in the analysis with a denser mesh in the air gap. Figure 3 shows the modeled thrust magnetic bearing

The flux path and the maximum load capacity were observed when maximum current was applied to the coils. Other parameters of interest are the inductance, slew rate and magnetic energy. The circuit model developed earlier assumes that all the magnetic flux generated by the coils passes across the air gap. However, all actuators will have some flux which does not cross the gap, generally leaking directly from the sides of one pole to the sides of an adjacent pole. These effects are captured by the finite element model.

Inductance is not directly available from the finite element solution. However, the inductance can be found from the total magnetic field energy, *W*, produced by the maximum current. The inductance can then be calculated as [10][]:

$$L_c = \frac{2W}{I^2} \tag{8}$$

2.2 Radial magnetic bearing

An inside out E-core type radial magnetic bearing is designed for the flywheel as depicted in **Error! Reference source not found.** In this design, the rotating part of the bearing is the outer ring. The bearing poles, windings, and the back iron are inside of the rotating ring and are on the stator. The E-core arrangement has four quadrants. An example quadrant is shown in Figure 4(b). The main pole in the center has about twice the pole face area as the two auxiliary poles. The bearing has a total of 12 poles.

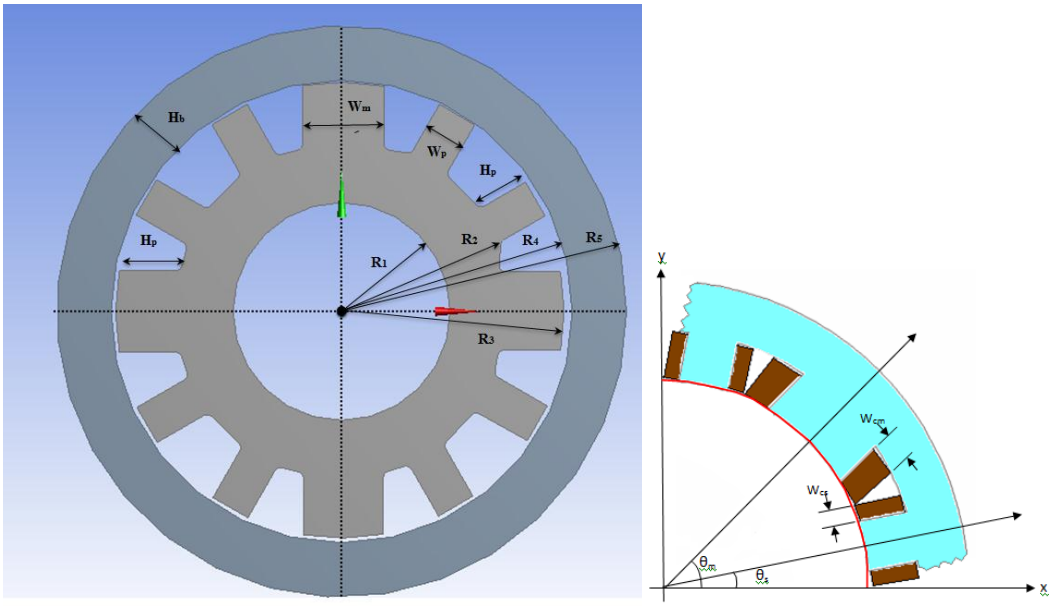

Figure 4 (a) Inside out E-core magnetic bearing (b) E-core magnetic bearing showing coil widths

The corresponding linear circuit for a single quadrant is shown in Figure 5 [9]. It is assumed that the magnetic flux is contained within each quadrant. Each quadrant has two magnetic flux loops.

2.2.1 Linear Circuit model

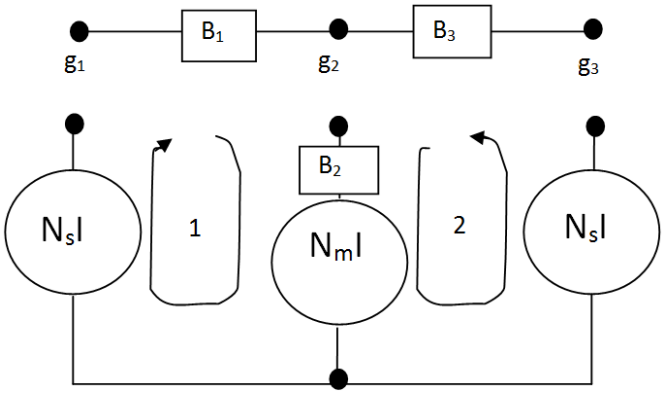

Figure 5 E-core Linear Magnetic Circuit Model [9]

The load capacity (F_{load}) of the radial bearing is calculated based on the rotor unbalance me_u. The unbalance level is based on residual unbalance levels recommended by API 617 [].

$$me_u = 6350\frac{W}{N} \tag{9}$$

In Eq. (9), the unbalance level me_u is expressed in g-mm. The weight of the rotor W is in kg, and the running speed N is in rpm. The units are not consistent, but the unbalance level is driven by specification. The resulting unbalance force amplitude is then given by:

$$F = (SF)me_u\Omega^2 \tag{10}$$

$$U = 6350\frac{W}{N}\ (g - mm) \quad (1).$$

The Eight Edition of API 617 will require a maximum safety factor of 12 for vibration limit checks.

The design radial force for one quadrants of the e-core bearing is found from [9]

$$F_{design} = \frac{A_{pm} B_{knee}{}^{2}[1+\sin(45^{o}+\theta_{s})]}{2\mu_{o}} \quad (11)$$

Assuming equal flux density in all of the poles, the flux density can be found in terms of air gap g, number of main pole turns N_m, and side pole turns N_s-as:

$$B = \frac{\mu_o (N_m + N_s) I}{2g} \quad (12)$$

Similar to the thrust bearing calculations performed in the previous section, the corresponding values of flux and current densities were taken. The three coils of each e-core are wound in series and the auxiliary poles have half the cross-sectional area of the main poles, the inductance for the circuit is given by [9]:

$$L = \frac{\mu_0 A_p (N_m + N_a)^2}{2g} \quad (13)$$

And the slew rate can be computed as

$$S = 2\frac{\left[1+\sin(56.37^{\circ})\right]}{g}\sin(45^{\circ})\, I_b V_c \quad (14)$$

Equations (9–14) were used to size the radial magnetic bearing.

2.2.2 Finite Element analysis:

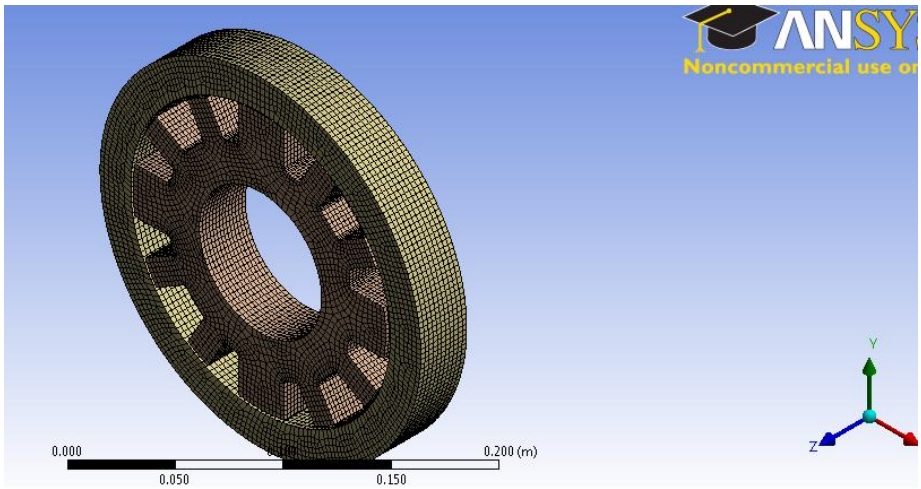

Figure 6 Radial magnetic bearing model

Because the circuit model assumes linear magnetic properties, the location and extent of saturation must be evaluated with finite element analysis (FEA). As with the case of the thrust bearing, an FEA was conducted to verify

the load capacity, flux path and flux density while deducing parameters such as inductance, magnetic energy and slew rate. The E-core model is shown in Figure 6. The inductance was computed based on Eq. (8).

3. Results

3.1 Thrust magnetic bearing

The different parameters computed from the linear circuit model analysis are listed in Table 1. It should be noted that the design flux density was taken as 1.2T. This is a typical linear B-H flux limit for silicon iron alloys. Also, a packing factor of 0.7 was applied in computing the coil cavity dimensions. The packing factor accounts for unused space with round wire winding and wire insulation. The packing factor results in an increased volume when calculating the magnetic bearing size. A 14AWG wire was used for the analysis.

Notation	Parameter	Value
m	Mass of the flywheel	50 kg
SF	Safety Factor	3
F_{Design}	Load capacity	1500N
B_{Knee}	Maximum flux density	1.2 T
I_{max}	Maximum current in coil	10 A (based on amplifier)
I_b	Bias current in coil	5 A
g_0	Nominal air gap	1.5 mm
d	Stator inner diameter	70 mm
d_a	Stator outer diameter	300 mm
h	Stator thickness	50 mm
N	Number of turns	288 turns
x	Width of coil cavity	20 mm
l_c	Length of coil cavity	105 mm

Table 1: Thrust magnetic bearing parameters

Finite Element Analysis

A two-dimensional thrust bearing model was developed in ANSYS using the dimensions calculated with the linear circuit model. This was done to verify the model before performing a full 3 dimensional analysis The peaks obtained in Figure 7 correspond to the flux density as observed in the air gap.

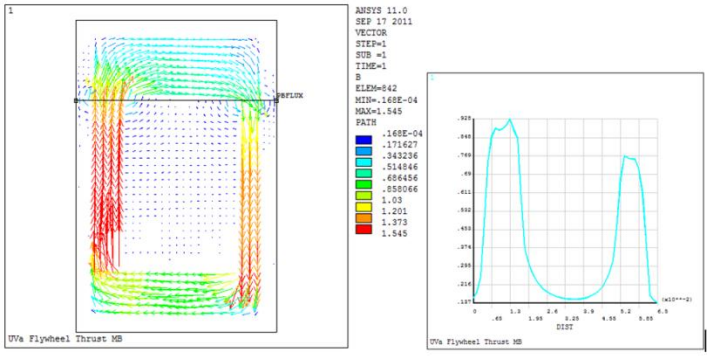

Figure 7: 2D Flux path and peaks for thrust bearing

The outputs studied in the 3D analysis were primarily the load capacity, flux density and the flux path. Figure 8 and Figure 9 show the results obtained from ANSYS. It should be noted that the flux density peaked at about 1.24 T with the obtained load capacity of 1800 N. The force of the same magnitude (but opposite direction) was found on the thrust disk and well as the stator.

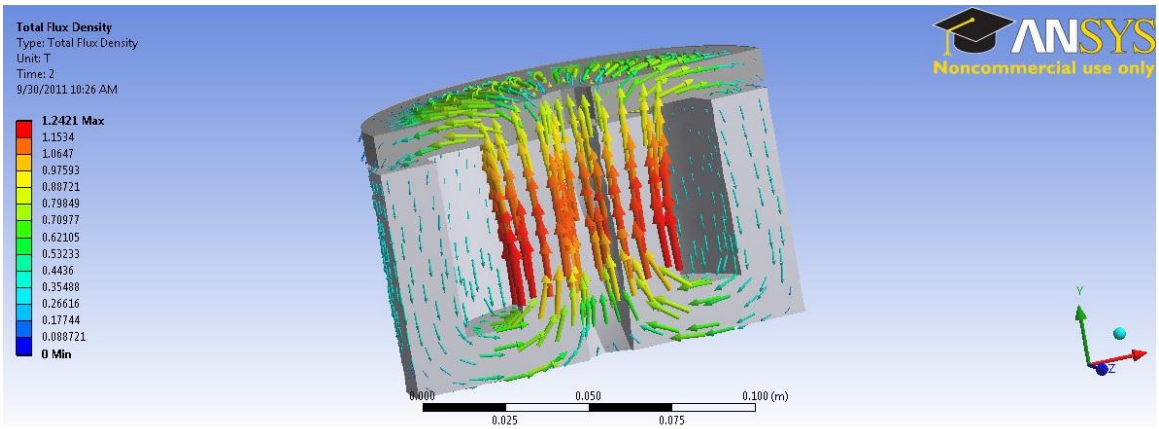

Figure 8: Flux path and total flux density of magnetic thrust bearing

The finite element model can also be used to estimate the leakage and improve the inductance calculation, which is a measure of the total magnetic field energy produced by a given current. The table below shows a comparison between the linear model and the FEA values obtained.

Analysis method	Force (N)	Magnetic energy (J)	Inductance (mH)	Force Slew rate (N/s)
Circuit Model	1500	-	68.1	$3.9 * 10^6$
FEA	1812	3.82	74.5	$3.2 * 10^6$

Table 2. Comparison of thrust bearing parameters

The inductance predicted by the finite element model was 9 percent higher than what was predicted by the linear circuit model. This led to a corresponding decrease in force slew rate predicted by the finite element model when compared to the linear circuit model. However, the load capacity prediction in the finite element model was significantly higher than the linear circuit model prediction.

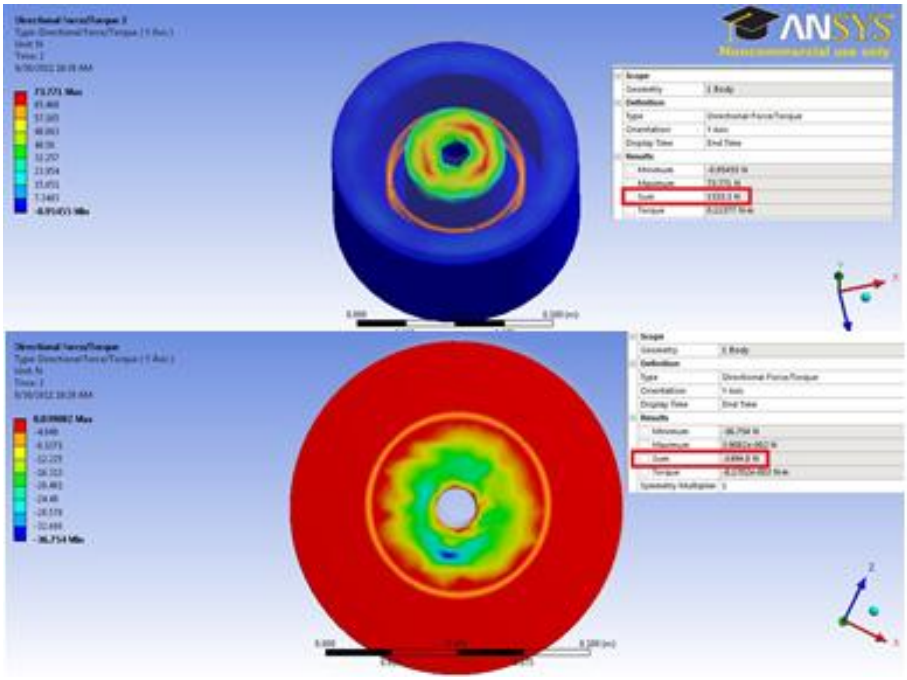

Figure 9: Force obtained from design on thrust stator and thrust disk

3.2 Radial magnetic bearing

The different parameters computed from the linear circuit model analysis of the e-core radial bearing are listed in Table 3. As with the thrust bearing, the design flux density was taken as 1.2T, and a packing factor of 0.7 was applied in computing the coil cavity dimensions. A 14AWG wire was used in the analysis.

Notation	Description	Value
W_m	Width of main pole	40 mm
W_s	Width of side pole	20 mm
W_{cm}	Core width on main pole	12.5mm
W_{cs}	Core width on side pole	6.25mm
L	Bearing axial length	92 mm
H_b	Height of back iron	33.5 mm
H_p	Height of radial pole	33.5 mm
H_c	Height of wounded coil	24 mm
H_l	Height of rotor lamination	30mm
R_1	Inner radius of Stator	35mm
R_2	Coil space radius	68.5mm
R_3	Outer radius of stator	101 mm
R_4	Inner radius of rotor laminations	102mm
R_5	Outer radius of rotor laminations	132mm
θ_m	Main pole centerline angle	45^o
θ_s	Side pole centerline angle	11^o
A_{pm}	Main pole cross sectional area	$3680mm^2$
A_{ps}	Side pole cross sectional area	$1840mm^2$
A_{cm}	Coil cross sectional area on main pole	$418.75mm^2$
A_{cs}	Coil cross sectional area on side pole	$209.375mm^2$
N_m	Number of turns on main pole	134
N_s	Number of turns on side pole	67
g	Air gap	1 mm
I_{max}	Max current in coil	10A

Table 3 Calculated design parameters of radial magnetic bearing

Finite Element Analysis

A 3D finite element magnetic analysis was done to verify the load capacity, flux path and flux density as in the case of the thrust bearing. Having verified the model for errors a mesh convergence study was done to ensure that enough elements were selected for the analysis. About 1 million elements were used for the analysis. Figure 10 and Figure 11 show the results obtained from ANSYS. It should be noted that the flux density peaked at about 1.6 T at maximum current with the load capacity of 990 N.

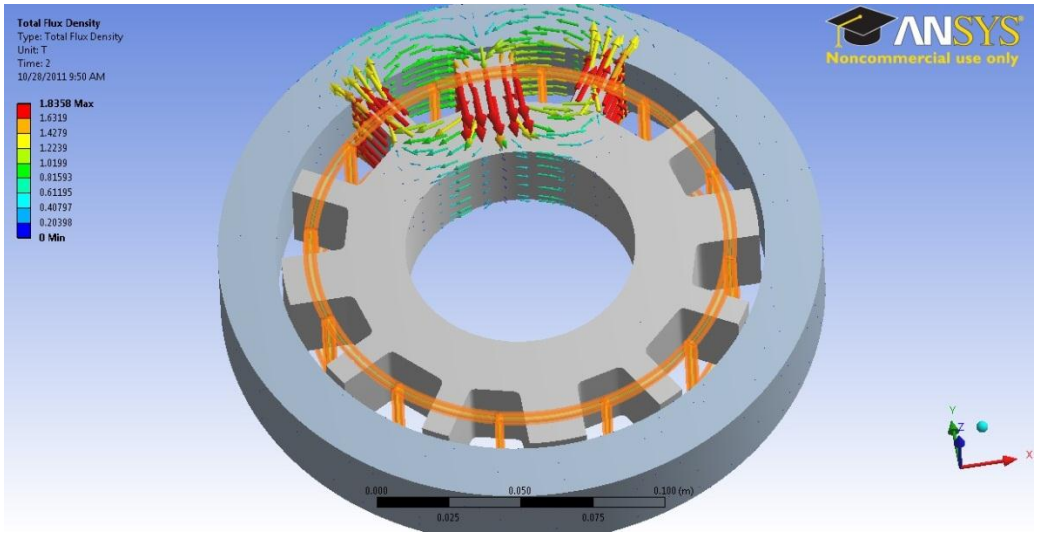

Figure 10: Flux path and total flux density of magnetic radial bearing

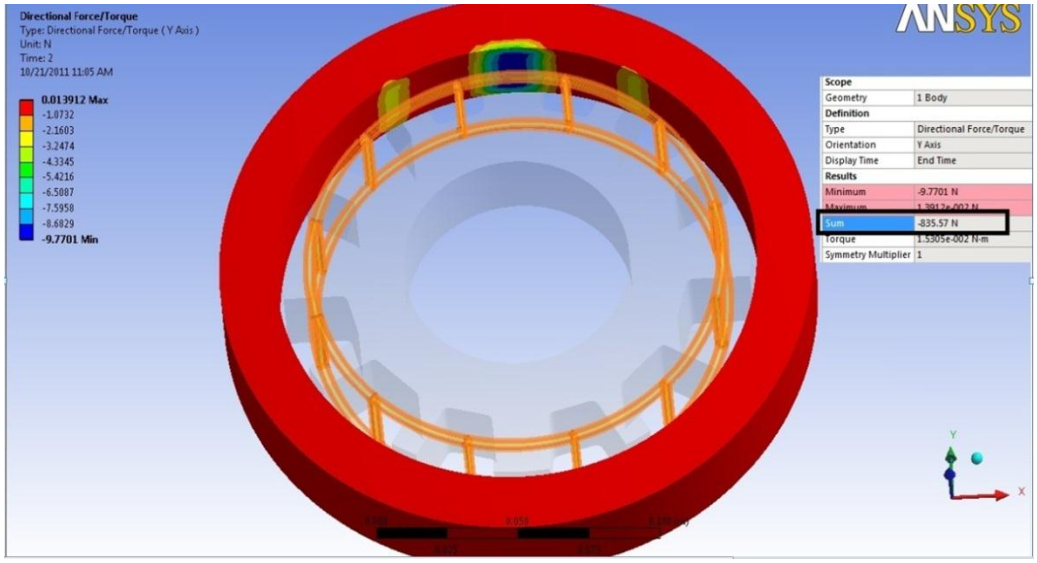

Figure 11 : Force obtained from 3D model on radial bearing laminations

The table below shows a comparison between the linear model and the FEA values obtained in calculations of inductance slew rate and load capacity

Analysis method	Force (N)	Magnetic energy (J)	Inductance (mH)	Force Slew rate (N/s)
Circuit Model	840	-	92.4	$7.1 * 10^6$
FEA	990	4.68	101.2	$6.4 * 10^6$

Table 4 Comparison of radial magnetic bearing parameters

As with the thrust bearing, the inductance predicted by the radial bearing finite element model was about 9 percent higher than that predicted by the linear circuit model. This resulted in a corresponding drop in force slew rate. The load capacity predicted by the finite element model was also higher than that predicted by the linear circuit model. However, the FEA predicted a peak flux of 1.6 T, which is entering the saturation region of silicon iron alloys. Additional work is required to ensure that the bearing will still operate in the linear range.

4 Conclusions

This study discusses the design of a thrust and radial magnetic bearing for a flywheel energy storage system. This flywheel energy storage system is under development at the University of Virginia and comprises of two radial bearings and a double-acting thrust bearing.

The design procedure for both the thrust and radial magnetic bearings was similar. Firstly, the load capacity was calculated, from which the required pole surface area could be found. The air gaps, maximum current in the amplifier, inner and outer diameters of the stator along with their thickness were chosen based on which the number of coil turns, length and width of a pole and other parameters were calculated. Finally, these values were input in ANSYS and a 3 dimensional model was created. The flux path along with the load capacity was visualized to check if they match with the calculated values. It should be noted that both these techniques yielded similar results. The parameters such as flux path, flux leakage, saturation and non-linear effects were taken into account in the 3-D model making it a much more accurate technique.

The required load capacity of the thrust bearing was based on the weight of the flywheel while that of the radial bearing was calculated based on the rotor unbalance. Parameters such as slew rate, magnetic energy and inductance were compared between the linear and FEA models. When compared to the finite element models, the linear circuit models had lower predictions for load capacity, inductance, and a higher prediction of slew rate.

References

[1] R Hebner, J Beno, A Walls. Flywheel batteries come around again, Spectrum, IEEE. 39 (2002) 46-51.

[2] H Liu, J Jiang. Flywheel energy storage—An upswing technology for energy sustainability, Energy Build. 39 (2007) 599-604.

[3] H Ibrahim, A Ilinca, J Perron. Energy storage systems--Characteristics and comparisons, Renewable and Sustainable Energy Reviews. 12 (2008) 1221-1250.

[4] E Reedy Jr, Composite-rim flywheel design, 1 (1977).

[5] L Hawkins, P MCMULLEN, R LARSONNEUR, Development of an AMB Energy Storage Flywheel for Commercial Application, (2005).

[6] JA Kirk, PA Studer. Flywheel energy storage--II:: Magnetically suspended superflywheel, Int.J.Mech.Sci. 19 (1997) 233-245.

[7] JG Bitterly. Flywheel technology: past, present, and 21st century projections, Aerospace and Electronic Systems Magazine, IEEE. 13 (1998) 13-16.

[8] B Bolund, H Bernhoff, M Leijon. Flywheel energy and power storage systems, Renewable and Sustainable Energy Reviews. 11 (2007) 235-258.

[9] P Tsao, M Senesky, SR Sanders. An integrated flywheel energy storage system with homopolar inductor motor/generator and high-frequency drive, Industry Applications, IEEE Transactions on. 39 (2003) 1710-1725.

[10] T Nehl, F Fouad, N Demerdash. Determination of saturated values of rotating machinery incremental and apparent inductances by an energy perturbation method, Power Apparatus and Systems, IEEE Transactions on. (1982) 4441-4451.

[11] API Standard 617, Axial and Centrifugal Compressors and Expander-compressors for Petroleum, Chemical,and Gas Industry Service, Downstream Segment, 7th ed., American Petroleum Institute,Washington, DC. (2002)